

Spectroscopy of annular drums and quantum rings: perturbative and nonperturbative results

Carlos Alvarado

*Facultad de Ciencias, Universidad de Colima,
Bernal Díaz del Castillo 340, Colima, Colima, Mexico*

Paolo Amore*

*Facultad de Ciencias, CUICBAS, Universidad de Colima,
Bernal Díaz del Castillo 340, Colima, Colima, Mexico*

We obtain systematic approximations to the states (energies and wave functions) of quantum rings (annular drums) of arbitrary shape by conformally mapping the annular domain to a simply connected domain. Extending the general results of Ref. [1] we obtain an analytical formula for the spectrum of quantum ring of arbitrary shape: for the cases of a circular annulus and of a Robnik ring considered here this formula is remarkably simple and precise. We also obtain precise variational bounds for the ground state of different quantum rings. Finally we extend the Conformal Collocation Method of [1, 2] to the class of problems considered here and calculate precise numerical solutions for a large number of states (≈ 2000).

PACS numbers: 02.30.Mv, 02.70.Jn, 03.65.Ge

I. INTRODUCTION

This paper extends the general results obtained in a recent paper by one of us, ref. [1], for simply connected drums and quantum billiards to domains with a hole, i.e. annular drums or quantum rings. Quantum rings are two dimensional regions of annular shape where an electron is confined and possibly subject to an external field (magnetic or electric); as for the simply connected case studied in ref. [1], only few special cases may be solved exactly, such as for the circular annulus, where the solutions may be expressed in terms of Bessel functions of first and second kind. However, quantum rings of general shape, for which exact solutions are not known, present interesting physical behaviors, thus justifying the effort of finding analytical or numerical approximations.

For instance, it is known that the bendings of an infinite wire cause the appearance of bound states below the continuum threshold [3] and of localized states in quantum rings in correspondence of regions of maximum curvature [4]. In particular, Gridin and collaborators have formulated in Ref. [4] an asymptotic approximation to the modes of a quantum ring, based on the assumption that the ratio of the ring half-width to the radius of curvature is small. Their approach extends to ring like domain the classical Keller-Rubinow method [5, 6]

In this paper we adopt a completely different strategy, which is both systematic and simple, and which can be used to obtain precise analytical and/or numerical approximations for the energies and eigenfunctions of a given quantum ring. The approach that we propose is

based on a generalization of the methods described in Ref. [1] and allows one to solve Helmholtz equation for the quantum ring of arbitrary shape by conformally mapping the ring to a simply connected domain. The results obtained in this way are very precise and prove to be useful even for the exactly solvable circular ring: in this case we have found an extremely precise formula for the energies of the rings, which avoids the use of Bessel functions and their zeroes.

It is important to underline that the method that we propose is systematic and that it can be applied to rings of arbitrary width and curvature.

The paper is organized as follows: in Section II we describe the numerical implementation of our method, using the Conformal Collocation Method of [1, 2]; in Section III we discuss the extension of the analytical techniques of [1] to the case of annular domains; in Section IV we apply the methods, both analytical and numerical, to the solvable problem of a circular annulus and to the less tractable problem of a "Robnik's ring", i.e. a ring whose external border corresponds to the family of quantum billiards studied by Robnik in [7] and known as "Robnik's billiards". Finally in Section V we summarize our results and draw our conclusions.

II. CONFORMAL COLLOCATION METHOD

In this section we describe the application of the Conformal Collocation Method (CCM) of Ref. [1, 2] to the solution of Schrödinger equation in a quantum ring. Although this approach has been already described in detail in those papers, we briefly review it here to make the discussion self-contained and to highlight the modifications which are needed to implement the specific problem at hand.

*Electronic address: paolo.amore@gmail.com (corresponding author)

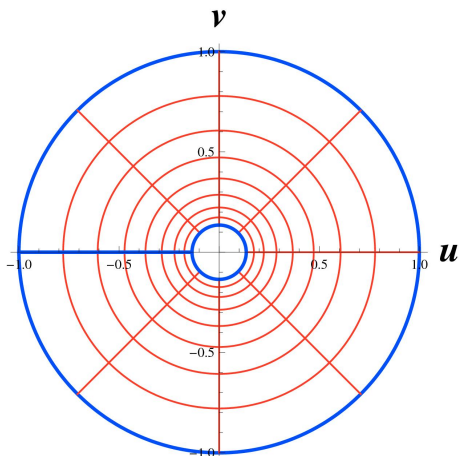


FIG. 1: (color online) Annulus obtained conformally mapping a rectangle of sides $2L_x = 2$ and $2L_y = 2\pi$ centered in the origin.

Our starting point is the homogeneous Helmholtz equation on a "ring-like" domain \mathcal{D} , which can be conformally mapped to an inhomogeneous Helmholtz equation on a "simpler" domain Ω , which is assumed here to be a rectangle. Let $w = f(z)$ where $w = u + iv$ and $z = x + iy$ ($(u, v) \in \mathcal{D}$ and $(x, y) \in \Omega$).

As a result one is left to work with the inhomogeneous Helmholtz equation on Ω :

$$-\frac{1}{\Sigma(x, y)} \Delta \psi(x, y) = E \psi(x, y). \quad (1)$$

where $\Sigma \equiv \left| \frac{df}{dz} \right|^2$.

An explicit example of conformal map with the desired properties is clearly the exponential map

$$f(z) = e^{z-L_x}, \quad (2)$$

which maps a rectangle of sides $2L_x$ and 2π centered in the origin into an annulus of radii e^{-2L_x} and 1 respectively. Fig. 1 displays the annulus obtained mapping a rectangle of sides $L_x = 2$ and $L_y = 2\pi$ centered in the origin (clearly using a smaller L_y one would obtain an arc instead of the full ring). Notice that the function of eq. (2) maps the horizontal sides into the horizontal segment which cuts the ring on the negative axis. This is clearly a different situation from those considered in Ref. [1]: as a matter of fact in this case the direct approach of Ref. [1] would describe an annulus with a straight cut on which Dirichlet boundary conditions are obeyed. Although this is also an interesting problem in itself, we want here to treat a ring with no cuts.

The solution to this problem is obtained by imposing periodic (Dirichlet) boundary conditions on the horizontal (vertical) sides of the rectangle. Under the conformal

map of eq. (2) the rectangle is then mapped into an annulus fulfilling Dirichlet boundary conditions on the smaller and larger circles. To implement the new boundary conditions in the problem we thus need to introduce a proper set of Little Sinc Functions (LSF): this set corresponds to LSF_1 of Ref. [8].

We report here the explicit form of the LSF_1 :

$$s_k^{(I)}(N, L, x) = \frac{(-1)^k \sin\left(\frac{(N+1)\pi x}{2L}\right)}{(N+1) \sin\left(\frac{\pi x}{2L} - \frac{\pi k}{N+1}\right)} \quad (3)$$

with $k = -N/2, \dots, N/2$. Notice that we use here a different convention for N with respect to Ref. [8]. These functions define the homogeneous grid $x_k = \frac{2Lk}{N+1}$ and satisfy the orthogonality relation

$$\int_{-L}^{+L} s_k^{(I)}(N, L, x) s_j^{(I)}(N, L, x) dx = \frac{2L}{N+1} \delta_{kj}. \quad (4)$$

Notice that $h^{(I)} \equiv \frac{2L}{N+1}$ is the grid spacing of the LSF_1 .

The LSF_2 fulfilling Dirichlet boundary conditions may be cast in the form

$$s_k^{(II)}(N, L, x) = \frac{(-1)^k \cos\left(\frac{\pi k}{N}\right) \sin\left(\frac{N\pi x}{2L}\right)}{N \sin\left(\frac{\pi x}{2L}\right) - \sin\left(\frac{\pi k}{N}\right)}. \quad (5)$$

with $k = -N/2+1, \dots, N/2-1$ ¹. In this case these functions define the homogeneous grid $x_k = \frac{2Lk}{N}$ and obey the orthogonality relation

$$\int_{-L}^{+L} s_k^{(II)}(N, L, x) s_j^{(II)}(N, L, x) dx = \frac{2L}{N} \delta_{kj}. \quad (6)$$

Notice that $h^{(II)} \equiv \frac{2L}{N}$ is the grid spacing of the LSF_2 .

For a given N (even integer) there are $N+1$ ($N-1$) LSF functions obeying periodic (Dirichlet) boundary conditions, each peaked (with value 1) at a point x_k and vanishing at the remaining grid points x_j , $j \neq k$.

A function $f(x)$ obeying periodic bc may be interpolated using the $s_k^{(I)}(h, N, x)$ as

$$f(x) \approx \sum_{k=-N/2}^{N/2} f(x_k) s_k^{(I)}(h, N, x). \quad (7)$$

Similarly we may derive twice this expression to obtain

$$\frac{d^2 f(x)}{dx^2} \approx \sum_{k=-N/2}^{N/2} f(x_k) \frac{d^2 s_k^{(I)}(x)}{dx^2}$$

¹ The reader may check that the expression given here for these functions is equivalent to the one used before in Ref. [1]

$$\begin{aligned}
&\approx \sum_{k=-N/2}^{N/2} \sum_{j=-N/2}^{N/2} f(x_k) \left. \frac{d^2 s_k^{(I)}(x)}{dx^2} \right|_{x_j} s_j^{(I)}(h, N, x) \\
&\equiv \sum_{k=-N/2}^{N/2} \sum_{j=-N/2}^{N/2} f(x_k) c_{kj}^{(I2)} s_j^{(I)}(h, N, x), \quad (8)
\end{aligned}$$

where in the last line we have introduced the matrix $c_{kj}^{(I2)} \equiv \left. \frac{d^2 s_k^{(I)}(x)}{dx^2} \right|_{x_j}$, which provides a representation for the second derivative operator on the grid. The case of Dirichlet bc has already been discussed in Ref. [1], although it can be obtained straightforwardly repeating the same steps done here. To take into account the presence of different sets of LSF we modify the notation of Ref. [1] and call $c_{kj}^{(I2)}$ the matrix elements of the second derivative obtained with Dirichlet bc. Notice that the latin indices k, j span different values in the two cases and that the grid points also differ in the two cases.

Omitting some trivial steps (see Ref. [1] for more detail) we may now easily discretize eqn. (1) using Dirichlet bc in the x direction and periodic bc in the y direction. A suitable "basis" for this discretization is obtained with the direct product of the LSF in each direction:

$$\begin{aligned}
& - \frac{1}{\Sigma(x, y)} \Delta s_k^{(II)}(h, N, x) s_{k'}^{(I)}(h, N, y) = - \sum_{jj'} \frac{1}{\Sigma(x_j, y_{j'})} \\
& \times \left[c_{kj}^{(II2)} \delta_{k'j'} + \delta_{kj} c_{k'j'}^{(I2)} \right] s_j^{(II)}(h, N, x) s_{j'}^{(I)}(h, N, y) \quad (9)
\end{aligned}$$

where it is understood that the latin indices span different ranges for the two LSF.

To obtain the matrix element of the operator on the grid we need to associate a single integer to any pair of indices which define an element of the two dimensional grid. We may write:

$$k = K - (N - 1) \left[\frac{K}{N - 1 + \epsilon} \right] - \frac{N}{2} \quad (10)$$

$$k' = -\frac{N}{2} + \left[\frac{K}{N - 1 + \epsilon} \right], \quad (11)$$

where $\epsilon \rightarrow 0^+$ and $[a]$ means integer part of a . In this way we are able to identify a point of the grid in terms of a single integer K , which takes values from 1 to $N^2 - 1$.

Using these relations we may read off the matrix element of \hat{O} as

$$O_{KK'} = -\frac{1}{\Sigma(x_j, y_{j'})} \left[c_{kj}^{(II2)} \delta_{k'j'} + \delta_{kj} c_{k'j'}^{(I2)} \right]. \quad (12)$$

Although the procedure described above uses grid with the same N for the x and y direction, a more appropriate choice is to use meshes with the same grid size on each orthogonal direction, i.e. $h^{(I)} \approx h^{(II)}$. In this way we may establish the relation between the number of grid points on each direction

$$N_x \approx \frac{L_x}{L_y} (N_y + 1).$$

We may easily understand the physics contained in this relation: for thin rings, $L_x \ll L_y$, the number of grid points in the x -direction is much less than the number of grid points in the y -direction, since the excitation of trasverse modes requires much higher energy than the excitation of longitudinal modes.

In this case one can extend the previous relations for the grid to:

$$\begin{aligned}
k &= K - (N_x - 1) \left[\frac{K}{N_x - 1 + \epsilon} \right] - \frac{N_x}{2} \\
k' &= -\frac{N_y}{2} + \left[\frac{K}{N_x - 1 + \epsilon} \right].
\end{aligned}$$

The implementation of these considerations allows us to represent the differential operator as a $(N_x - 1)(N_y + 1) \times (N_x - 1)(N_y + 1)$ hermitean matrix.

It is useful to summarize the differences with the results of Ref. [1]:

- The region Ω is a rectangle of sides $2L_x$ and $2L_y$, where $L_y = \pi$ to allow a closed ring
- The operator \hat{O} is represented on the grid by a $(N_x - 1)(N_y + 1) \times (N_x - 1)(N_y + 1)$ hermitean matrix
- The collocation points, corresponding to the nodes of the LSF functions, differ for the x and y directions: on the x direction they are distributed following the zeroes of the LSF with Dirichlet boundary conditions, while on the y direction they are distributed following the zeroes of the LSF with periodic boundary conditions. Their numbers (N_x and N_y) are also different, although the grid size is (approximately) the same.

Apart from these small differences, the remaining features of the collocation method are unchanged. In particular, the matrix representing \hat{O} on the grid is obtained from the product of a diagonal matrix, representing $1/\Sigma$ on the grid, with a non-diagonal sparse matrix, representing the Laplacian with mixed bc on the grid. While the first matrix is specific to the problem considered and therefore it needs to be calculated each time that a different shape is chosen, the second matrix is universal and therefore it can be calculated and stored once and for all. As before the calculation of the diagonal matrix is not computationally demanding since it just requires the evaluation of the function $1/\Sigma$ at the $(N_x - 1)(N_y + 1)$ points forming the grid.

We will illustrate later specific applications of the CCM.

III. ANALYTICAL METHODS

In this section we generalize the analytical approach of Ref. [1] to describe quantum rings. We may consider two

different approaches: in the first one the quantum ring is obtained performing a conformal map of a rectangle centered in the origin (as described in the previous section); in the second one the quantum ring is obtained by applying a conformal map directly to a circular annulus.

While the formulas of Ref. [1] hold both cases, one needs to work with different orthonormal basis in the two cases.

In the first case where Ω is a rectangle of sides $2L_x$ and 2π , the basis is obtained by the direct product of functions obeying Dirichlet and periodic boundary conditions, i.e.

$$\psi_{n_x}(x) = \frac{1}{\sqrt{L_x}} \sin\left(\frac{n_x\pi}{2L_x}(x + L_x)\right) \quad (13)$$

for the Dirichlet bc and

$$\chi_0(y) = \frac{1}{\sqrt{2\pi}}, \quad (14)$$

$$\chi_{n_y}(y) = \frac{1}{\sqrt{\pi}} \cos(n_y y), \quad (15)$$

$$\phi_{n_y}(y) = \frac{1}{\sqrt{\pi}} \sin(n_y y), \quad (16)$$

for the periodic bc. Notice that $n_{x,y} = 1, 2, \dots$

The basis on Ω may then be written as

$$\Psi_{n_x, n_y, s}(x, y) = \psi_{n_x}(x) \times \begin{cases} \chi_{n_y}(y) & , s = 1 \\ \phi_{n_y}(y) & , s = 2 \end{cases} ,$$

where the value $n_y = 0$ can only be reached for the states with $s = 1$.

In the second case, the wave function of a circular annulus with $a < r < b$ is (see for example Ref. [9])

$$\begin{aligned} \Phi_{m,n,s}(r, \theta) = N_{mns} & \left[Y_m(k_{mn}) J_m\left(\frac{k_{mn}r}{a}\right) \right. \\ & \left. - J_m(k_{mn}) Y_m\left(\frac{k_{mn}r}{a}\right) \right] \times \begin{cases} \cos n\theta & , s = 1 \\ \sin n\theta & , s = 2 \end{cases} , \end{aligned}$$

where J_m and Y_m are Bessel functions of first and second kind and k is the n^{th} root of the equation

$$Y_m(k) J_m\left(\frac{kb}{a}\right) - J_m(k) Y_m\left(\frac{kb}{a}\right) = 0. \quad (17)$$

The energies of the annulus are then given by

$$E_{mn} = \left(\frac{k_{mn}}{a}\right)^2, \quad m = 0, 1, 2, \dots, \quad n = 1, 2, \dots \quad (18)$$

where

$$\begin{aligned} \Delta_{n_x, n_y, s, n'_x, n'_y, s'}(k, j) & \equiv \int_{-L_x}^{+L_x} dx \int_{-\pi}^{+\pi} dy \Psi_{n_x, n_y, s}(x, y) (e^{x-L_x})^{(k+j)+2} \cos(y(k-j)) \Psi_{n'_x, n'_y, s'}(x, y) \\ & = \alpha_{n_y} \alpha_{n'_y} \delta_{ss'} W_{n_x, n'_x}(k, j) \mathcal{I}_{n_y, n'_y, k, j}^{(s)}, \end{aligned} \quad (22)$$

Although one may work equally well with each of the two basis, from the point of view of an analytical calculation the first one offers the advantage of simplicity, since it involves only elementary functions. We will therefore focus on this basis.

We consider the most general conformal transformation which maps the rectangle Ω onto a ring of arbitrary shape:

$$g(z) = C \sum_{k=0}^{\infty} \eta_k (e^{z-L_x})^{k+1} \equiv C \bar{g}(z), \quad (19)$$

where $\eta_0 = 1$ and $C > 0$ is a constant factor, representing a dilation. The energies of the ring obtained using the mapping $g(z)$ (E_n) are related to those of the ring obtained using $\bar{g}(z)$ (\bar{E}_n) by the simple relation²

$$E_n = \frac{\bar{E}_n}{C^2}.$$

We may therefore work with $\bar{g}(z)$ and then simple rescale the energies obtained.

Notice also that with the choice $C = 1$ and $\eta_{k>0} = 0$ we obtain the map to the circular annulus considered earlier.

With simple algebra we obtain the conformal density

$$\begin{aligned} \Sigma(x, y) & \equiv \left| \frac{d\bar{g}}{dz} \right|^2 = \sum_{k=0}^{\infty} \sum_{j=0}^{\infty} \eta_k \eta_j (k+1)(j+1) \\ & \cdot (e^{x-L_x})^{(k+j)+2} \cos(y(k-j)) \end{aligned} \quad (20)$$

and $\sigma(x, y) = \Sigma(x, y) - 1$.

As discussed in Ref. [1] we need to calculate the matrix elements of σ between the states of Ω . We find:

$$\begin{aligned} \langle n_x, n_y, s | \sigma(x, y) | n'_x, n'_y, s' \rangle & = -\delta_{n_x, n'_x} \delta_{n_y, n'_y} \delta_{ss'} \\ & + \sum_{k=0}^{\infty} \sum_{j=0}^{\infty} \eta_k \eta_j (k+1)(j+1) \Delta_{n_x, n_y, s, n'_x, n'_y, s'}(k, j) \end{aligned} \quad (21)$$

and $\alpha_0 = 1/\sqrt{2\pi}\delta_{s,1}$ and $\alpha_{n_y>0} = 1/\sqrt{\pi}$.

We have also introduced the definitions

$$\begin{aligned} W_{n_x, n'_x, k, j} &\equiv \int_{-L_x}^{+L_x} \psi_{n_x}(x) (e^{x-L_x})^{(k+j)+2} \psi_{n'_x}(x) dx \\ &= \frac{8\pi^2 L_x n_x n'_x (j+k+2) e^{-2L_x(j+k+2)} \left((-1)^{n_x+n'_x} e^{2L_x(j+k+2)} - 1 \right)}{(4L_x^2 (j+k+2)^2 + \pi^2 (n_x - n'_x)^2) (4L_x^2 (j+k+2)^2 + \pi^2 (n_x + n'_x)^2)} \end{aligned} \quad (23)$$

and

$$\begin{aligned} \mathcal{I}_{n_y, n'_y, k, j}^{(1)} &\equiv \int_{-\pi}^{+\pi} \cos(n_y y) \cos(n'_y y) \cos((k-j)y) dy \\ &= \frac{\pi}{2} \left[\delta_{n_y - n'_y + (k-j)} + \delta_{n_y + n'_y + (k-j)} + \delta_{n_y - n'_y - (k-j)} + \delta_{n_y + n'_y - (k-j)} \right] \\ \mathcal{I}_{n_y, n'_y, k, j}^{(2)} &\equiv \int_{-\pi}^{+\pi} \sin(n_y y) \sin(n'_y y) \cos((k-j)y) dy \\ &= \frac{\pi}{2} \left[\delta_{n_y - n'_y + (k-j)} - \delta_{n_y + n'_y + (k-j)} + \delta_{n_y - n'_y - (k-j)} - \delta_{n_y + n'_y - (k-j)} \right]. \end{aligned} \quad (24)$$

Notice that the $\mathcal{I}_{n_y, n'_y, k, j}^{(s)}$ have been already defined in Ref. [1]; the reader should also observe that there are no terms mixing states with different values of s and that $\mathcal{I}_{n_y, n'_y, k, j}^{(1)} = \mathcal{I}_{n_y, n'_y, k, j}^{(2)}$ unless $n_y + n'_y = \pm(k-j)$.

We may understand the physical consequences of these properties by considering the approximate expression for the energy:

$$\bar{E}_{n_x, n_y, s} \approx \frac{\epsilon_{n_x, n_y, s}}{\langle n_x, n_y, s | \Sigma(x, y) | n_x, n_y, s \rangle}, \quad (25)$$

where

$$\epsilon_{n_x, n_y, s} \equiv \frac{n_x^2 \pi^2}{4L_x^2} + n_y^2 \quad (26)$$

With simple algebra we obtain

$$\begin{aligned} \langle n_x, n_y, s | \Sigma(x, y) | n_x, n_y, s \rangle &= \sum_{k=0}^{\infty} \sum_{j=0}^{\infty} \eta_k \eta_j (k+1)(j+1) \left[W_{n_x, n_x, k, k} \delta_{k,j} + (-1)^{s+1} W_{n_x, n_x, k, j} \delta_{2n_y - |k-j|} \right] \\ &= \sum_{k=0}^{\infty} \eta_k^2 (k+1)^2 W_{n_x, n_x, k, k} + (-1)^{s+1} \sum_{k=2n_y}^{\infty} \eta_k \eta_{k-2n_y} (k+1)(k+1-2n_y) W_{n_x, n_x, k, k-2n_y} \\ &\quad + (-1)^{s+1} \sum_{k=0}^{\infty} \eta_k \eta_{k+2n_y} (k+1)(k+1+2n_y) W_{n_x, n_x, k, k+2n_y}, \end{aligned} \quad (27)$$

where the terms depending explicitly on s will be respon-

are the "unperturbed" energies (i.e. the energy on the rectangle Ω).

This expression has been derived in Ref. [1] resumming specific terms in the perturbative expansion corresponding to a geometric series: it has later been applied in Ref. [10] to obtain a Weyl-like law for inhomogeneous drums.

sible of the breaking of the degeneration of levels.

IV. APPLICATIONS

We will now consider few applications of the numerical and analytical techniques developed here and in Ref. [1] to quantum rings of different shape.

A. Circular annulus

Our first application is to the calculation of the energies and wave functions of the circular annulus using the basis of the rectangle.

We may use eq. (25) and obtain an explicit formula for the energies of a circular annulus:

$$E_{n_x, n_y, s} \approx \frac{2 (\log^2(a) + \pi^2 n_x^2) (n_y^2 \log^2(a) + \pi^2 n_x^2)}{\pi^2 (a^2 - 1) n_x^2 \log(a)} \quad (28)$$

where $a = e^{-2L_x}$ is the inner radius of the ring.

Notice that the states corresponding to $n_y = 0$ are non-degenerate, whereas the states corresponding to $n_y > 0$ are doubly degenerate: in other words the basis that we are using reproduces the exact pattern of degeneration of the circular annulus.

In Fig. 2 we compare the exact numerical results obtained solving eq. (18) (solid curve) with the results obtained using the analytical formula (28) (dashed curve) for the first 2000 states. The dotted line corresponds to the numerical results obtained using the CCM with a grid with $N_x = 14$ and $N_y = 400$ (remember that the ratio $N_x/(N_y + 1)$ should approximately be L_x/L_y). Finally the dot-dashed line are the results obtained using Weyl's law supplemented by Weyl's conjecture

$$E_n \approx \frac{4\pi n}{A} + \frac{L}{A} \sqrt{\frac{4\pi n}{n}} + \dots, \quad (29)$$

where A and L are area and perimeter of the ring respectively (Dirichlet boundary conditions are chosen).

Amazingly the first three curves are practically indistinguishable. In Fig. 3 we display the the error of the analytical formula, which is about 0.1 % for all the states considered.

We may also obtain precise results for the ground state of the ring using a variational approach. Following Ref. [1] we pick a trial state

$$|\chi\rangle = \sum_k c_k^{(0)} |k\rangle, \quad (30)$$

where $|k\rangle \equiv |k_x, k_y\rangle$ are eigenstates of the rectangle with mixed bc. Using the inverse operator \hat{O}^{-1} we may generate a new state

$$|\Psi_0^{(1)}\rangle = \hat{O}^{-1} |\chi\rangle, \quad (31)$$

which has a larger overlap with the true ground state of the system.

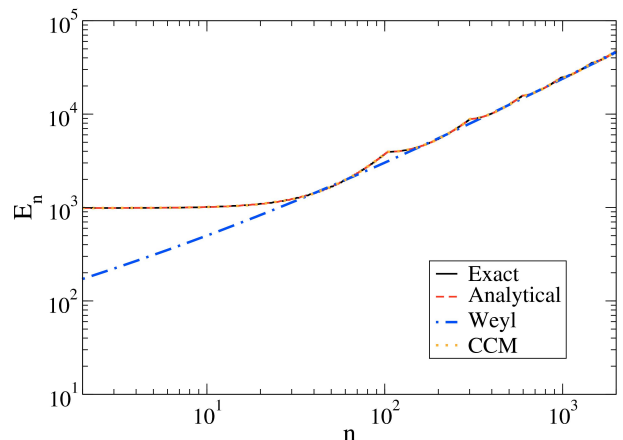


FIG. 2: (color online) Energy of the first 2000 states of an annulus with $a = 9/10$ and $b = 1$. The solid line are the exact results of eq. (18); the dashed line corresponds to eq. (28); the dotted line are the numerical results obtained with CCM; the dot-dashed line are the results obtained with Weyl's law supplemented by Weyl's conjecture.

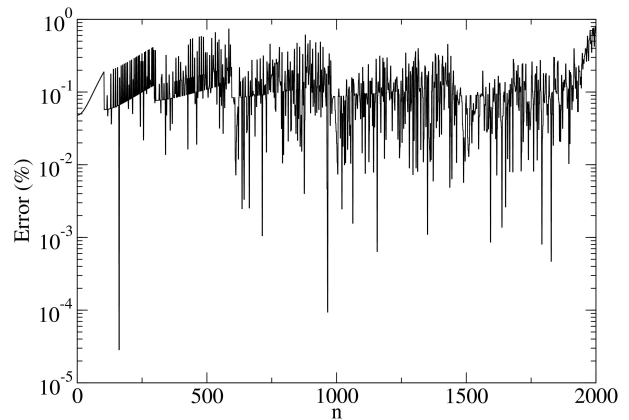


FIG. 3: (color online) Relative error of the analytical formula (28) with respect to the exact results

The expectation value of \hat{O} in this state is

$$E_0^{(1)} = \frac{\langle \Psi_0^{(1)} | \hat{O} | \Psi_0^{(1)} \rangle}{\langle \Psi_0^{(1)} | \Psi_0^{(1)} \rangle}, \quad (32)$$

where

$$\langle \Psi_0^{(1)} | \hat{O} | \Psi_0^{(1)} \rangle = \sum_{k,l,m=0}^{\infty} \frac{c_k^{(0)} c_m^{(0)}}{\epsilon_l} \langle m | \Sigma^{1/2} | l \rangle \langle l | \Sigma^{1/2} | k \rangle \quad (33)$$

$$\begin{aligned} \langle \Psi_0^{(1)} | \Psi_0^{(1)} \rangle &= \sum_{l, l', m, m'=0}^{\infty} \frac{c_m^{(0)} c_{m'}^{(0)}}{\epsilon_l \epsilon_{l'}} \langle m' | \Sigma^{1/2} | l' \rangle \langle l' | \Sigma | l \rangle \\ &\times \langle l | \Sigma^{1/2} | m \rangle. \end{aligned} \quad (34)$$

By minimizing $E_0^{(1)}$ with respect to the coefficients $c_k^{(0)}$ one can now find precise estimates for the ground state energy. Let us now pick a specific trial state. We will work in the limit of an annulus with $(b-a) \ll 1$, which corresponds to using $L_x \ll 1$.

We use the trial state

$$\begin{aligned} |\chi\rangle &= c_0^{(0)} \psi_1(x) \chi_0(y) \\ &+ \psi_1(x) \sum_{n_y=1}^N \left[c_{2n_y-1}^{(0)} \phi_{n_y}(y) + c_{2n_y}^{(0)} \chi_{n_y}(y) \right] \end{aligned} \quad (35)$$

neglecting in first approximation the excited states in the x direction.

We need to calculate the matrix elements

$$\begin{aligned} \langle m | \Sigma^{1/2} | l \rangle &= \langle 1, m_y | \Sigma^{1/2} | 1, l_y \rangle \\ &= \left[\int_{-L_x}^{+L_x} \psi_1^2(x) e^{x-L_x} dx \right] \delta_{m_y l_y} \\ &= \frac{\pi^2 e^{-L_x} \sinh(L_x)}{L_x^2 + \pi^2} \delta_{m_y l_y} \end{aligned} \quad (36)$$

$$\begin{aligned} \langle m | \Sigma | l \rangle &= \langle 1, m_y | \Sigma | 1, l_y \rangle \\ &= \left[\int_{-L_x}^{+L_x} \psi_1^2(x) e^{2x-2L_x} dx \right] \delta_{m_y l_y} \\ &= \frac{\pi^2 (1 - e^{-4L_x})}{4(4L_x^2 + \pi^2)} \delta_{m_y l_y} \end{aligned} \quad (37)$$

Therefore

$$E_0^{(1)} = \frac{\sum_k \frac{(c_k^{(0)})^2}{\epsilon_k} \left[\frac{\pi^2 e^{-L_x} \sinh(L_x)}{L_x^2 + \pi^2} \right]^2}{\sum_k \frac{(c_k^{(0)})^2}{\epsilon_k^2} \left[\frac{\pi^2 e^{-L_x} \sinh(L_x)}{L_x^2 + \pi^2} \right]^2 \frac{\pi^2 (1 - e^{-4L_x})}{4(4L_x^2 + \pi^2)}} \quad (38)$$

Therefore we may write the matrix elements:

$$\begin{aligned} \langle m | \Sigma^{1/2} | l \rangle &= \langle m_x, 0 | \Sigma^{1/2} | l_x, 0 \rangle = \left[\int_{-L_x}^{+L_x} \psi_{m_x}(x) \psi_{l_x}(x) e^{x-L_x} dx \right] \\ &= \begin{cases} \frac{\pi^2 e^{-L_x} m_x^2 \sinh(L_x)}{L_x^3 + \pi^2 L_x m_x^2} & , m_x = l_x \\ \frac{8\pi^2 e^{-2L_x} L_x m_x l_x (e^{2L_x} - (-1)^{m_x+l_x}) \cos(\pi(m_x+l_x))}{16L_x^4 + 8\pi^2 L_x^2 (m_x^2 + l_x^2) + \pi^4 (m_x^2 - l_x^2)^2} & , m_x \neq l_x \end{cases} \\ \langle m | \Sigma | l \rangle &= \langle m_x, 0 | \Sigma | l_x, 0 \rangle = \left[\int_{-L_x}^{+L_x} \psi_{m_x}(x) \psi_{l_x}(x) e^{2x-2L_x} dx \right] \\ &= \begin{cases} \frac{\pi^2 e^{-4L_x} (e^{4L_x} - 1) m_x^2}{4(4L_x^3 + \pi^2 L_x m_x^2)} & , m_x = l_x \\ \frac{16\pi^2 e^{-4L_x} L_x l_x m_x (e^{4L_x} - (-1)^{l_x+m_x}) \cos(\pi(l_x+m_x))}{256L_x^4 + 32\pi^2 L_x^2 (l_x^2 + m_x^2) + \pi^4 (m_x^2 - l_x^2)^2} & , m_x \neq l_x \end{cases} \end{aligned} \quad (41)$$

Notice that in this case $\epsilon_n = \frac{\pi^2 n^2}{4L_x^2}$.

where

$$\epsilon_k = \frac{\pi^2}{4L_x^2} + \left[\frac{k+1}{2} \right]^2 \quad (39)$$

where $\left[\frac{k}{2} \right]$ is the integer part of $k/2$. Since one of the coefficients $c_k^{(0)}$ can be chosen arbitrarily we may pick $c_0^{(0)} = 1$ and minimize $E_0^{(1)}$ with respect to the remaining coefficients. The result is $c_k^{(0)} = 0$, for $k \geq 1$, which is equivalent to working with eq. (25). This fact should not be surprising, since the states corresponding to non-vanishing $c_k^{(0)}$ (for $k \geq 1$) break the rotational invariance of the true ground state of the annulus and therefore they must raise the energy. This explains the very good precision of eq. (28) for annuli with $b-a \gg 1$.

To improve this formula for states with smaller inner radius we may form a variational trial state with a superposition of wave functions in the x direction:

$$|\chi\rangle = \phi_0(y) \sum_{n_x=1}^N c_{n_x}^{(0)} \psi_{n_x}(x) \quad (40)$$

In Table I we report the ground state energy of the annulus calculated using the variational principle, i.e using the variational formula (38) together with eq. (40), with different numbers of variational parameters. The case $N = 1$ corresponds to the simple analytical formula (28), which is seen to work very well for larger values of a . It is easy to understand why more and more terms are needed as a gets smaller and smaller: since L gets larger, the conformal map strongly deforms the radial coordinate in the annulus. Looking at Fig. 1, which corresponds to

$a = 1/e^2$, we observe that the radial grid spacing is finer for smaller values of r . Therefore one needs more terms in eq. (38) to obtain good estimates of the energy. Notice that this argument also holds for the Conformal Collocation Method, since also the collocation points are also distributed non-uniformly in the radial direction, as the central hole is made smaller.

| a | $N = 1$ | $N = 2$ | $N = 3$ | $N = 4$ | $N = 5$ | $N = 10$ | exact |
|----------|-------------|-------------|-------------|-------------|-------------|-------------|-------------|
| 1/100000 | 24.74037682 | 13.58247813 | 10.13874976 | 8.585413233 | 7.763566890 | 6.639748109 | 6.493374419 |
| 1/10000 | 20.56383831 | 11.77986914 | 9.129597650 | 7.994645335 | 7.425906261 | 6.751169408 | 6.693191961 |
| 1/1000 | 16.67307038 | 10.21973107 | 8.409275276 | 7.691356864 | 7.367206060 | 7.062604524 | 7.048038125 |
| 1/100 | 13.49800490 | 9.359102734 | 8.360288280 | 8.036684452 | 7.920642510 | 7.846777753 | 7.845162680 |
| 1/10 | 13.31090873 | 11.31798812 | 11.04543198 | 10.99627372 | 10.98600010 | 10.98222952 | 10.98218981 |
| 1/2 | 39.81860401 | 39.03110135 | 39.01558313 | 39.01353082 | 39.01336954 | 39.01328910 | 39.01328850 |
| 9/10 | 987.1575032 | 986.6840018 | 986.6837734 | 986.6831548 | 986.6831530 | 986.6831306 | 986.6831305 |
| 99/100 | 98696.22334 | 98695.79206 | 98695.79206 | 98695.79151 | 98695.79151 | 98695.79149 | 98695.79149 |

TABLE I: Energy of the ground state of the annulus with varying inner radius calculated using the variational formula (38) together with eq. (40), with different numbers of variational parameters ($N - 1$ is the number of variational parameters). Notice that in this case $\epsilon_n = \frac{\pi^2 n_x^2}{4L_x^2}$.

In Fig. 4 we have plotted the exact energy of the ground state of the annulus as a function of the inner radius a and we have compared it with the different approximations considered earlier. The simple analytical formula of eq. (28) is seen to work quite well for thin annuli, while the most accurate variational calculation of Table I is seen to reproduce the exact results even for very small inner radiuses. We also report the CCM results corresponding to a grid with $N = 50$.

B. Robnik's rings

We consider the conformal map

$$f(z) = e^{-L_x + z} + \alpha e^{-2L_x + 2z} \quad (42)$$

which maps the rectangle of sides $2L_x$ and 2π into a deformed ring, which for $\alpha = 0$ has the shape of a circular ring and for $\alpha = 1/2$ has the shape of a cardioid ring. We have called the family of these annular billiards "Robnik's rings", in analogy with the simply connected billiards known as "Robnik's billiards" having the same external contour [7].

In this case we have:

$$\Sigma(x, y) = 4\alpha^2 e^{4x - 4L_x} + 4\alpha e^{3x - 3L_x} \cos(y) + e^{2x - 2L_x} \quad (43)$$

Notice that in this case the width of the ring is not uniform: we call r_{\mp} the smallest and largest width of the ring respectively, which read

$$r_{\pm} = \pm \alpha (1 - e^{-4L_x}) - e^{-2L_x} + 1. \quad (44)$$

Their average is insensitive to α :

$$\bar{r} \equiv \frac{r_+ + r_-}{2} = 1 - e^{-2L_x}. \quad (45)$$

Notice also that $1 - \bar{r} = e^{-2L_x} = a$ (in this case a is the average inner radius of the quantum ring).

Using the general results obtained earlier we may write the analytical formula:

$$E_{n_x, n_y, s} \approx \frac{2(\log^2(a) + \pi^2 n_x^2)(n_y^2 \log^2(a) + \pi^2 n_x^2)}{\pi^2 (a^2 - 1) n_x^2 \log(a) + \alpha^2 R_{n_x}(a)} \quad (46)$$

where

$$R_{n_x}(a) \equiv 2\pi^2 (a^4 - 1) n_x^2 \log(a) (\log^2(a) + \pi^2 n_x^2).$$

This formula reduces to eq. (28) for $\alpha = 0$.

In Fig.6 we display the energies of the first 2000 states of an annulus obtained conformally mapping a rectangle of sides $2L_x = 1/5$ and $2L_y = 2\pi$ with the map $f(z) = z + \alpha z^2$ using $\alpha = 1/10$. The solid line represents the precise numerical values obtained using CCM with a grid

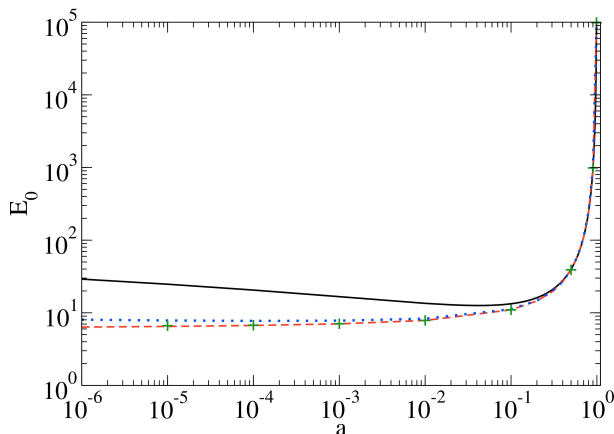


FIG. 4: (color online) Ground state energy of the annulus as a function of the inner radius keeping the outer radius fixed ($b = 1$). The dashed line is the exact result, while the dashed line is the analytical formula of eq. (28). The dotted line is the result obtained using CCM with $N = 50$; the pluses are the variational results of Table I corresponding to $N = 10$.

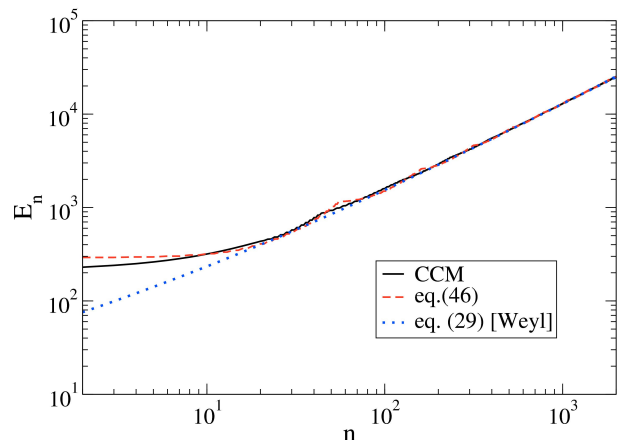


FIG. 6: (color online) Energies of the first 2000 states of an annulus obtained conformally mapping a rectangle of sides $2L_x = 1/5$ and $2L_y = 2\pi$ with the map $f(z) = z + \alpha z^2$ using $\alpha = 1/10$. The solid line are the numerical results obtained using CCM; the dashed line corresponds to the analytical formula, the dotted line is Weyl's law.

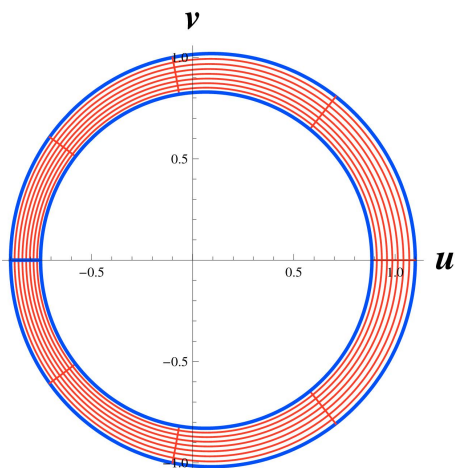


FIG. 5: (color online) Asymmetric annulus obtained conformally mapping a rectangle of sides $2L_x = 1/5$ and $2L_y = 2\pi$ centered in the origin. $\alpha = 1/10$.

with $N_x = 14$ and $N_y = 400$; the dashed line corresponds to the results of the analytical formula of eq. (46); finally, the dotted line corresponds to Weyl's formula eq. (29). In Fig. 6 we display a detail of the previous figure, for highly excited states around $n = 2000$.

Looking at the figure we see that our analytical formula describes more accurately than Weyl's equation, eq. (29),

the low lying part of the spectrum, although the latter describes better the high part of the spectrum. We also notice that the analytical formula displays a behaviour already observed for the circular annulus: around specific n , corresponding to the opening of a new transversal mode, the curve displays a small change of slope. While this behaviour is correct for the circular annulus, where it is indeed observed, neither the numerical results nor (of course) Weyl's expression display such a behaviour. However we may easily understand the origin of it: the analytical formula eq. (46) is obtained using a resummation of the terms in the Rayleigh-Schrödinger series which contains only the expectation values of the conformal density in a given state. For the circular annulus, this approximation is quite good because there is no mixing between transversal and longitudinal modes as a result of the rotational symmetry of the domain: this is reflected in the amazing accuracy of the analytical formula in this case. For a general annulus, the domain is not invariant under rotation and transverse and longitudinal modes actually mix. Already to second order in perturbation theory, there are terms which allow this mixing, although these are not present in the resummed formula.

As a check of the quality of the numerical results obtained with the CCM we have applied a method devised by Berry, ref. [11], which allows one to extract the geometrical feature of a domain from a limited sequence of eigenvalues, using improved eigenvalues sums. For the area, for example, one obtains a family of approximating

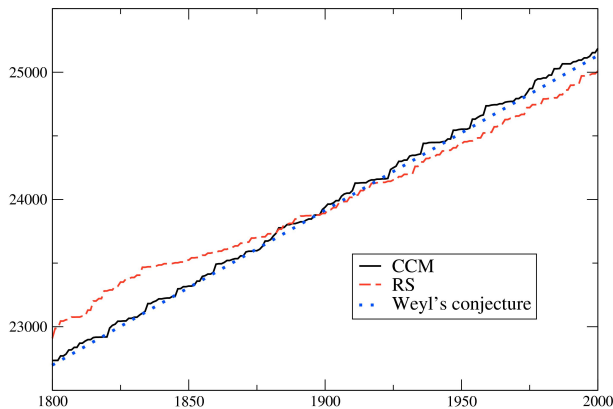


FIG. 7: (color online) Detail of the previous figure.

functions whose first few elements read [11]

$$A_0(t) = 4\pi t \sum_{n=0}^N e^{-E_n t} \quad (47)$$

$$A_1(t) = 4\pi t \sum_{n=0}^N e^{-E_n t} (2E_n t - 1) \quad (48)$$

$$A_2(t) = 4\pi t \sum_{n=0}^N e^{-E_n t} E_n t (2E_n t - 3) \quad (49)$$

$$A_3(t) = 4\pi t \sum_{n=0}^N e^{-E_n t} E_n t (4E_n^2 t^2 - 12E_n t + 3) / 3 \quad (50)$$

$$\dots = \dots \quad (51)$$

Analogous expressions are given in Ref. [11] for the length and constant terms in the asymptotic expansion of the function counting the number of states up to a given energy [12]

$$\langle n(E) \rangle \approx AE/4\pi - L\sqrt{E}/4\pi + C + \dots \quad (52)$$

The constant C should vanish for domains with one hole.

In figs.8,9 and 10 we have displayed the approximants for the area, perimeter and for the constant term built using the first 2000 numerical eigenvalues obtained with the CCM with a grid 14×400 . The horizontal lines are the exact values.

To estimate the optimal value of t where the approximant should be evaluated we minimize the sum of the squares of the derivatives of each approximant. For example, for the area we minimize the quantity $A_1'(t)^2 + A_2'(t)^2 + A_3'(t)^2$ (we leave out $A_0(t)$ because it is clearly less precise). For the length and constant terms we use the approximants displayed in the figures.

As shown in Table II the method of Berry allows us to extract the area, perimeter and constant terms of the

| | A | L | C |
|---------------------|---------|---------|----------|
| method of Ref. [11] | 1.07027 | 11.5221 | -0.01738 |
| exact | 1.07032 | 11.5250 | 0 |

TABLE II: Estimates for the geometrical features of the annulus obtained conformally mapping a rectangle of sides $2L_x = 1/5$ and $2L_y = 2\pi$ with the map $f(z) = z + \alpha z^2$ using $\alpha = 1/10$ using the method of Berry,[11] on the numerical results obtained with the CCM. The last row contains the exact results.

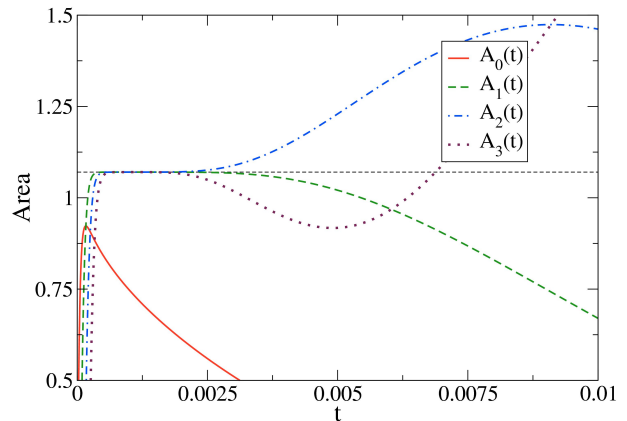


FIG. 8: (color online) Area approximant functions $A_m(t)$ for the first 2000 eigenvalues obtained with CCM with a grid 14×400 .

annulus with a truly amazing precision. Notice that the exact values of the area and perimeter are obtained directly using the conformal density:

$$A = \int_{\Omega} dx dy \Sigma(x, y) \quad (53)$$

$$L = \int_{\partial\Omega} ds \sqrt{\Sigma(x, y)}, \quad (54)$$

where Ω is the rectangle of sides $2L_x = 1/5$ and $2L_y = 2\pi$ and $\partial\Omega$ is the border of Ω where Dirichlet bc are obeyed³.

As we did before, we may also resort to a variational calculation and use the trial state:

$$|\chi\rangle = c_0^{(0)} \psi_1(x) \chi_0(y) + \psi_1(x) \sum_{n_y=1}^N \left[c_{2n_y-1}^{(0)} \phi_{n_y}(y) + c_{2n_y}^{(0)} \chi_{n_y}(y) \right] \quad (55)$$

neglecting in first approximation the excited states in the x direction. In the case of the circular ring we have seen

³ In ref. [10] these relations are used to derive Weyl's law from perturbation theory.

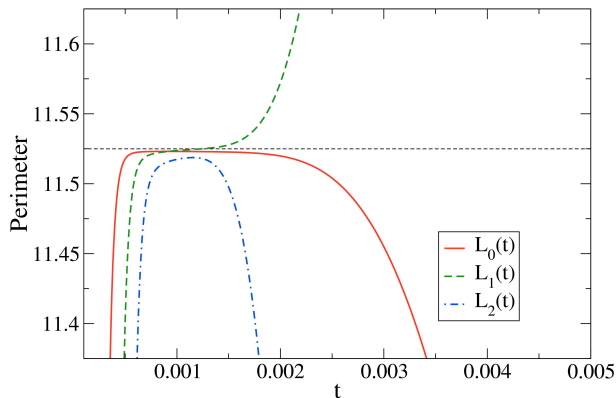


FIG. 9: (color online) Length approximant functions $L_m(t)$ for the first 2000 eigenvalues obtained with CCM with a grid 14×400 .

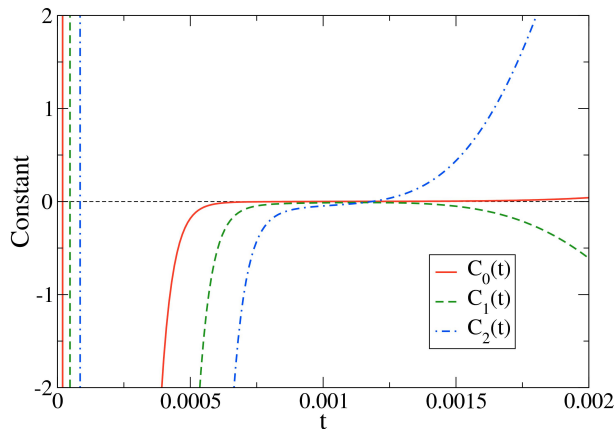


FIG. 10: (color online) Constant approximant functions $C_m(t)$ for the first 2000 eigenvalues obtained with CCM with a grid 14×400 .

that only the first term contributes, due to the rotational invariance of the ground state; this limit corresponds to the simple formula (25), which was seen to work remarkably well for thin circular rings.

In the present case we do not expect that the lowest order formula work well even for thin rings, due to the varying width of the ring, which favors the breaking of the rotational invariance.

We may apply this variational calculation to the Robnik annulus that we have considered before, which corresponds to $\alpha = 1/10$ and $L_x = 1/10$, shown in Fig. 5. In

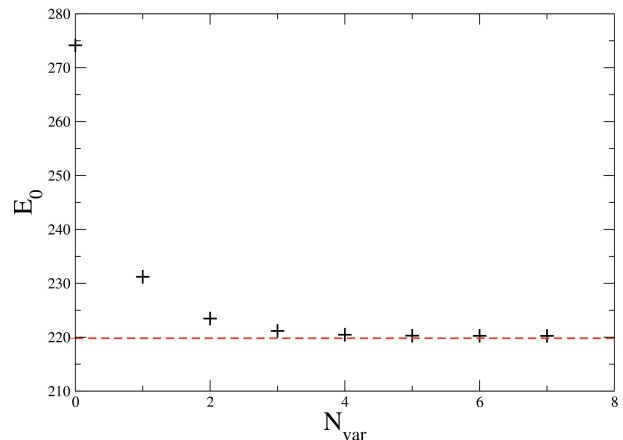


FIG. 11: (color online) Energy of the ground state of the asymmetric annulus with $L_x = 1/10$ and $\alpha = 1/10$. The horizontal line is the precise numerical value obtained with the CCM with a grid with 14×400 ; the pluses are the variational results obtained with a varying number of variational parameters.

this case we have

$$r_- = 0.148, \quad r_+ = 0.214. \quad (56)$$

In Fig. 11 we show the variational estimates for the ground state energy of this ring obtained using a varying number of variational parameters N_{var} (the case $N_{var} = 0$ corresponds to the simple analytical formula (25)); the horizontal line is the precise value obtained with the Conformal Collocation method with a grid with $N = 100$. As anticipated, the eq. (25) in this case provides a poor approximation to the exact energy, leading to a substantial overestimation of it. On the other hand, the inclusion of few longitudinal modes leads to quite drastic improvement, which can be already appreciated for $N_{var} = 2$. We should point out that, even letting $N_{var} \Rightarrow \infty$ (assuming that we can perform the calculation), we do not expect that the variational energy converge to the exact energy: the reason of this is that the variational ansatz that we are using includes only longitudinal modes (in the y direction) while completely neglecting the trasversal ones (in the x direction). For thin rings, the latter are less important, and therefore we are able to obtain good (but not arbitrarily good) approximations; for thick rings, on the other hand, only the inclusion of both modes will lead to acceptable approximations.

Finally in Fig. 12 we have plotted the wave function of the ground state of this annulus: as anticipated, this wave function is not invariant under arbitrary rotations and it is peaked in the region where the ring is wider, as expected. The wave function is multiplied by a factor 10

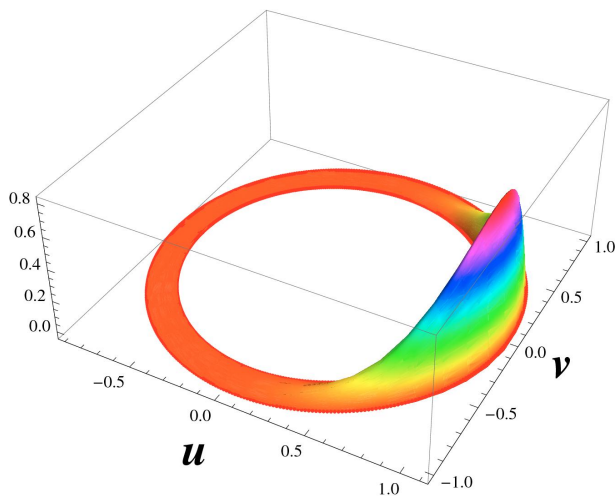


FIG. 12: (color online) Wave function (multiplied by a factor of 10) of the ground state of the Robnik's annulus with $L_x = 1/10$ and $\alpha = 1/10$.

to better appreciate the localization in the region where the width of the annulus is larger.

V. CONCLUSIONS

In this paper we have extended the powerful techniques of Ref. [1, 10] to the study of quantum rings; working on specific examples we have obtained both numerical and analytical results of remarkable precision. In fact our approach provides a systematic tool for the study of the spectrum of quantum rings of arbitrary shape, not relying on specific assumptions concerning the shape or

the width of the ring. Clearly, the problem of finding the particular conformal map which sends the rectangle to a specific ring may be attacked numerically, when the explicit expression is unknown [13, 14].

The results that we obtain in the paper maybe roughly classified into:

- numerical results obtained using the Conformal Collocation Method (CCM) for a large number of levels (≈ 2000); the accuracy of these results has been verified using Berry's approximants to estimate the geometrical features of the rings with a selected number of levels, calculated numerically;
- variational estimates for the ground state of a quantum ring;
- explicit analytical formulas for the whole spectrum of a quantum ring; the relation of these formulas with Weyl's law is also obtained in light of the results of Ref. [10];

We believe that the importance of our methods thus relies in the possibility of describing with precision both the low and high end of the spectrum of a quantum ring and on the possibility of improving this precision in a simple and systematic fashion. To the best of our knowledge there are no other approaches in the literature which share these features.

Finally, we wish to mention that the approach that we have described here can be applied directly also to annular drums of variable density (for simply connected drums this has been done in Ref. [10]).

Acknowledgments

P. Amore acknowledges support of Conacyt through the SNI fellowship.

-
- [1] P. Amore, Spectroscopy of drums and quantum billiards: perturbative and non perturbative results, accepted on the Journal of Mathematical Physics, arXiv:0910.4798v1 [quant-ph] (2009)
- [2] P. Amore, Journal of Physics **A** 41, 265206 (2008)
- [3] J. Goldstone and R.L. Jaffe, Phys.Rev.**B** 45, 14100 (1992)
- [4] D. Gridin, A. T. I. Adamou, and R. V. Craster, Phys. Rev. **B** 69, 155317 (2004)
- [5] J.B. Keller and S.I. Rubinow, Ann. Phys. Leipzig **9**, 24 (1960)
- [6] J.B. Keller, SIAM Rev. **27**, 485 (1985)
- [7] M. Robnik, J. Phys.**A** 17, 1049-1074 (1984)
- [8] P. Amore, F.M.Fernández, K. Salvo and R.A. Saénz, J. Phys.**A**, 115302 (2009)
- [9] J.R. Kuttler and V.G. Sigillito, SIAM Review **26** (1984) 163-193
- [10] P. Amore, arXiv:0912.1402v1 [math-ph] (2009)
- [11] M.V.Berry, J. Phys.**A** 20, 2389-2403 (1987)
- [12] Baltes H P and Hilf E R 1976 Spectra of Finite Systems (Mannheim: B-I Wissenschaftsverlag)
- [13] T. A. Driscoll. A MATLAB Toolbox for Schwarz-Christoffel mapping, ACM Trans. Math. Soft. 22 (1996), pp. 168-186.
- [14] T. A. Driscoll. Algorithm 843: Improvements to the Schwarz-Christoffel Toolbox for MATLAB, ACM Trans. Math. Soft. 31 (2005), 239-251.